Design of Spoof Surface Plasmon Polariton-based Sensor for Low Dielectric Constant Liquid Samples

Ivana Podunavac, Vasa Radonic, Vesna Bengin, Nikolina Jankovic

Abstract—**In this paper we propose a sensing platform for dielectric constant sensing based on a microwave spoof surface plasmon polaritons sensor and integrated chamber for liquid samples. The influence of different geometrical parameters on sensor response are analyzed, and the sensor performances are optimized for ultrasensitive detection of low dielectric constant in liquid samples.**

Keywords—**Microwave sensor, Spoof surface plasmon polariton, Dielectric constant sensing.**

I. Introduction

Microwave sensors present a promising solution for a wide range of applications due to the possibility for non-destructive, non-contact, and real-time measurements that can be easily miniaturized and combined with other sensing components. Recently, microwave sensors have been proposed for applications in food quality control [1]-[2], detection of biomolecules [3], glucose monitoring [4], dielectric constant sensing [5]-[6] and biomedical applications [7]. At microwave frequencies interaction between electromagnetic (EM) field and polar nature of liquid molecules enables detection of conductive and dielectric properties of liquid samples. Therefore, microwave sensors have been successfully used for sensing of dielectric constant for liquid samples [7]-[9]. However, many of the sensors do not have the ability to detect a small difference in dielectric constants, and they are usually proposed for detection in a wide range of values, i.e., for applications that do not require precise detection.

One of the promising phenomena that enable sensitive response in miniaturized devices is surface plasmon polariton (SPP) propagation [10]. SPP are surface waves that propagate at the conductor/dielectric interface, induced by the interaction between incident light and surface carriers of the conductor at optical frequencies. Many unique optical properties of SPPs such as localized field enhancement and light confinement at the subwavelength scale enabled the realization of miniaturized and highly sensitive sensors

suitable for refractive index sensing [11]-[13], protein measurements [14], and sucrose concentration [15]. However, at far-infrared, microwave, and terahertz frequencies, metals behave like perfect electric conductors (PEC) and therefore, do not the support propagation of SPPs. In order to mimic SPP propagation at microwave and terahertz frequencies, the concept of spoof surface plasmon polaritons (SSPPs) was introduced by using designed structures and plasmonic metamaterials [16]. Although the SSPP structures have a promising potential for sensing applications, only few such sensors were proposed in the literature [17]-[19].

In this paper, a SSPP-based microwave sensor with a novel design of unit cell is presented, and the influence of different geometrical parameters on sensor sensitivity and linearity are analysed. In addition, the optimized sensing platform is realized in rapid, cost-effective technology that combines xurography and laser micromachining processes, and sensing performances are experimentally confirmed with oil samples.

II. Analysis of the Structure

The layout of the proposed microwave SSPP-based sensor is presented in Fig. 1a. The array of unit cells (UCs) in the top and bottom layers (Layers 1 and 7) provides the SSPP propagation and dielectric constant sensing. In the conductive layers, arrays of UCs behave like an effective medium for EM waves that provide slow-wave behaviour in the frequency range that corresponds to the resonant behaviour of the unit cell. Therefore, the wave confinement occurs, and it can be observed by deviation from the light line in the dispersion diagram. Finally, the surface plasmon frequency in the dispersion diagram corresponds to the frequency of transmission zero in the response of the SSPP structure, when the propagation of the EM wave is not allowed.

Between two conductive layers, a sample reservoir is hosted in the dielectric materials (Polyvinyl Chloride (PVC) layers 2 and 6, Poly (methyl methacrylate)-PMMA – layer 4, and 3M double-sided adhesive tapes layers 3 and 5) and they host a sample reservoir closed from the top and bottom side. The fabrication and bonding of these layers will be described in the following section.

Ivana Podunavac, Vasa Radonic, Vesna Bengin and Nikolina Jankovic are with the BioSense Institute, University of Novi Sad, Dr Zorana Djindjica 1, 21000 Novi Sad, Serbia (e-mail: ivana.podunavac@biosense.rs, vasarad@biosense.rs, bengin@biosense.rs, nikolina@biosense.rs).
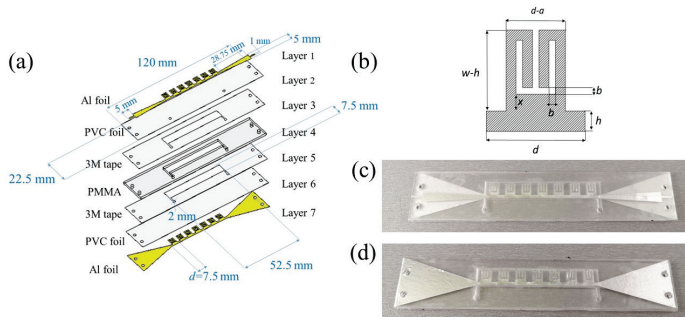
Fig. 1. (a) Multilayer structure of the SSPP-based sensor. (b) Proposed unit cell. (c) Top view of the realized sensor. (d) Bottom view of the realized sensor.

Fig. 2. Dispersion curve for periods of unit cell d= 2.5, 5, 7.5, and 10 mm. Inset: Positions of transmission zeros in the frequency specter for dielectric permittivity that correspond to sample with unit dielectric permittivity.

The modelling of the sensor has been done in CST Microwave Studio 2021®, where the following parameters are used for simulating materials. The 40-µm-thick Al layers are modelled with electrical conductivity of 3.56 x 10^7 S/m. The 80-µm-thick PVC foil is characterised with the dielectric constant of 3.3 and $tan\delta$ 0.15, while 2-mm-thick PMMA is modelled with the dielectric constant of 2.6 and $tan\delta$ 0.02. Although the 3M tape properties make a negligible contribution to the results, it is modelled as a thin film with dielectric constant 3.

Considering that the array of UCs is the core of the sensing principle that provides SSPP phenomena in the structure, sensor performances and linearity are examined for different values of the UC period. Also, we investigate how the number of unit cells influence losses in the structure.

The novel design of UC is proposed and characterised with the following parameters, which are the function of the period of UC d: distance between grooves a=0.4d, groove depth h=0.8d, structure width w=d, width of the bent structures b=0.67d, and distance between bent shapes and groove depth x=0.2(w-h). From the previous relations, it can be seen that all of the parameters are function of the UC period, and that the whole structure is being scaled by changing this parameter. The proposed design of UC is proved to be more compact in comparison with comb-shaped unit cell, [6].

First, we examine the sensor response for different values of the UC period. In that sense, Fig. 2 presents dispersion diagrams for the UC periods in the range from 2.5 mm to 10 mm for unit dielectric permittivity of the sample. The simulations of UC have been done by using *Eigenmode solver* for an infinite array of UCs. As it was mentioned previously, by changing the size of the UC period, the whole UC is being scaled, and therefore the range of frequencies that will be used for sensing can be adjusted to a specific frequency range. In that sense, from Fig. 2 it can be seen that the SSPP phenomena in larger structures, i.e., structures with higher values of the UC period, occurs at lower frequencies.

The inset of Fig. 2 shows the responses of the corresponding final sensor design, which contains an array of 7 UCs, and one can note that the deep and sharp transmission zeros correspond to the surface plasmon frequencies. The responses have been obtained using *Transient solver*.
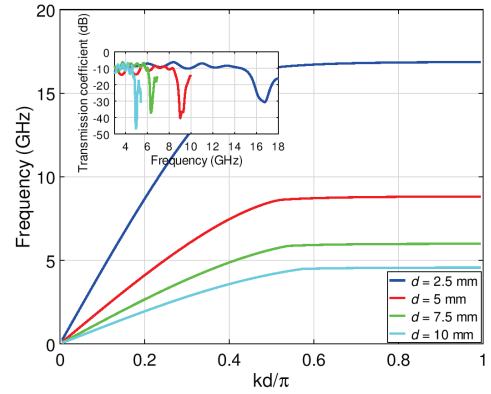
Considering that the final sensor structure will be used for sensing applications, an examination of sensor response, sensitivity, and linearity have been done for a sample dielectric constant in the range 1-5. Fig. 3 presents sensor responses for the UC period in the range 2.5 – 10 mm and different values of dielectric constants of samples. Table I summarizes all parameters of sensitivity and linearity for different UC periods. The sensitivity is calculated according to the expression $(f_{max}-f_{min})/(\varepsilon_{max}-\varepsilon_{min})$, where ε_{max} and ε_{min} are the maximum and minimum value of sample dielectric permittivity, while f_{max} and f_{min} are the transmission zero frequencies that correspond to the ε_{max} and ε_{min}, respectively.

It can be seen that the best linearity is obtained in the structure with the period of unit cell d=7.5 mm, namely R^2=0.964, while the sensitivity is 569 MHz/epsilon unit in the range of dielectric permittivity 1-5. Although structures with d=2.5, 5, and 10 mm show better sensitivity, good linearity properties are one of the most important properties for sensing applications.

TABLE I
COMPARISON OF SENSOR SENSITIVITY AND LINEARITY FOR DIFFERENT PERIODS OF UNIT CELLS

Period of unit cell [mm]	Sensitivity [MHz/epsilon unit]	Linearity R^2	Equation
2.5	757.5	0.8956	-0.718 ε + 16.982
5	718.8	0.962	-0.7124 ε + 9.486
7.5	532.1	0.964	-0.5633 ε + 6.7239
10	611.19	0.8932	-0.5772 ε + 5.7012

In the following simulation results, the UC period is fixed to d=7.5 mm due to its excellent linear properties and its compact dimensions. Further analysis comprises a comparison of the responses of the structures with different number of UCs. Namely, the dispersion diagrams and surface plasmon frequencies are obtain under the assumptions that the structure is infinite, while the realistic scenario allows only for a finite number of UCs. Therefore, one can expect discrepancies between the ideal and realistic cases and the analysis reveals the number of UCs that provide a good trade-off between the size of the structure and overall performance.
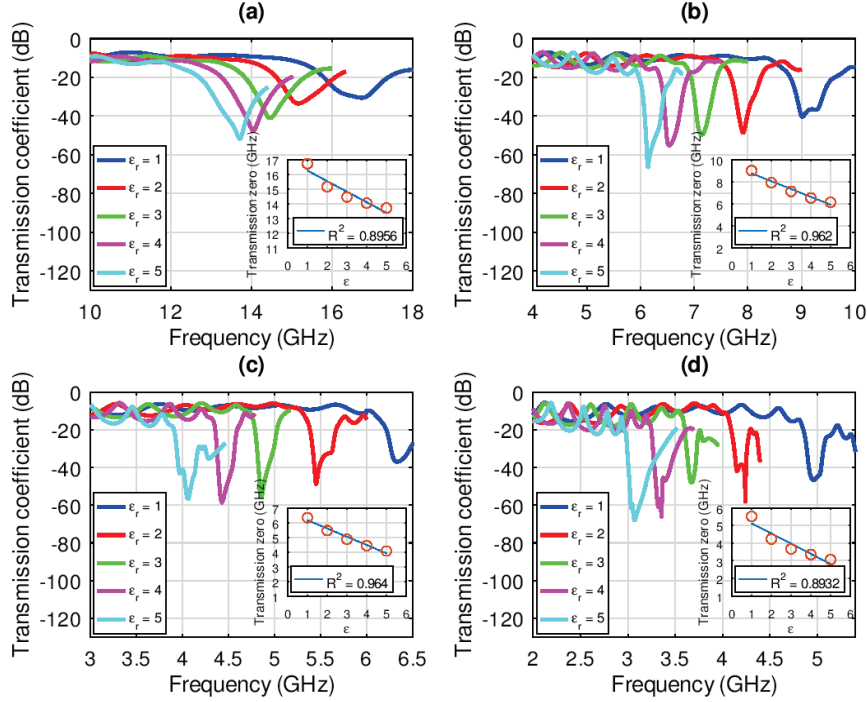
Fig. 3. Sensor response for low dielectric constant samples (a) d=2.5 mm, (b) d=5 mm, (c) d=7.5 mm, (d) d=10 mm.

Fig. 4 shows simulation results for the number of UCs 5, 7, and 9, for epsilon values 1, 3, and 5, where there is no significant difference in terms of transmission zero position, and consequently sensitivity potential. It can be seen that the structure with 9 UCs exhibits deeper transmission zeros in comparison with 5 and 7 UCs which showed similar behavior. On the other hand, Fig. 4 also shows that the number of UCs determines losses in the structure and shows that the structure with a lower number of UCs has lower losses. Consequently, 7 UCs have been chosen as a good trade-off between the size of the sensor and sufficiently deep transmission zeros to be detected in measurements, and low-loss properties.

III. FABRICATION AND TESTING OF SENSING PERFORMANCES

The optimized sensor design with UC period of 7.5 mm, and 7 UCs showed excellent linear properties of R^2=0.964, and good sensitivity of 532.1 MHz/epsilon unit in the range of dielectric constant 1-5, and it has been chosen to be fabricated and tested. The sensor structure has been manufactured in rapid, hybrid technology that combines laser micromachining and xurography. Layers 1 and 7 (Fig. 1a) with an array of 7 UCs have been realized in Al sticky foils and have been cut with Nd:YAG laser (Rofin-Sinar Power Line D-100). The integrated chamber for liquid samples is realized in Layer 4, which is closed from the top and bottom side with PVC foils (MBL 80MIC Belgrade, Serbia) (Layers 2 and 6). The PMMA has been cut with CO2 laser (CNC—MBL 4040RS), while designs of PVC foils and 3M double-sided tapes have been realized with Plotter Cutter (DG CAMM-1 GS-24) The cold lamination bonding of all layers has been done with 3M double sided adhesive tapes (Layers 3 and 5). Fig. 1c and d present the top and bottom views of the realized structure, respectively.
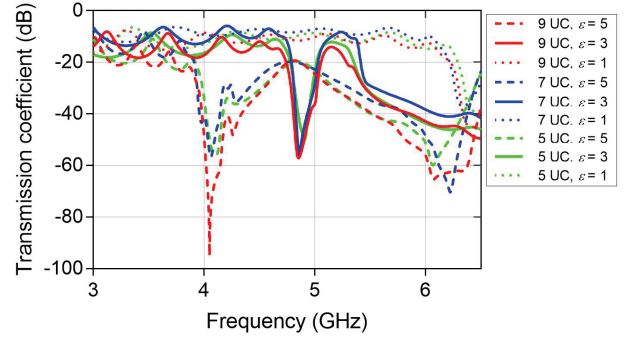

Fig. 4. Dispersion curve for periods of unit cell d= 2.5, 5, 7.5, and 10 mm. Inset: Positions of transmission zeros in the frequency specter for dielectric permittivity that correspond to air.

Testing of the sensor has been done with samples of oils that correspond to the range of dielectric constants used in simulations. The following samples have been used in measurements: sunflower oil (Edible Refined oil, Bas Bas, Serbia), olive oil (Cadel Monte, 100% Italian Extra Virgin), palm oil (Palm oil for frying, Dijamant, Serbia), and castor oils (Livsane, Serbia). The values of oil dielectric permittivities have been taken from the literature, which are listed in in Table II. The measurements have been done by filling the reservoir in the SSPP-based sensor with the oil samples, and consequent measurements of S-parameters using a vector network analyser (VNA) E5071C Agilent Technology. Surface mount assembly (SMA) connectors (SMA Southwest Microwave 292-04A-5) have been used for connection between VNA and SSPP sensor.

Table II presents the values of dielectric permittivities of oil samples from the literature, and the losses of oil samples estimated in the simulations for the value $tan\delta$ that best fits the experimental curve. The comparison between simulations

and experimental results is presented in Fig. 5a where the good overlapping between simulated and measured spectral positions of transmission zeros can be observed. The small differences in the spectrum can be attributed to the imperfection of fabrication procedure and losses in the cables and connectors in the experimental setup. Fig. 5b shows that in the range of oil dielectric constants 1.8 – 2, the sensor has excellent sensitivity of 850 MHz/epsilon unit and has shown excellent linearity (R^2=0.9918) in experimental measurements. The results have confirmed its strong potential for sensing and applications in oil quality control.

Although the fabrication procedure enables rapid fabrication of complex structures, the imperfections of realized structures are determined by the tool used for cutting, i.e., the laser beam. Its beam width can introduce small differences between modelled and realized structures which can cause small differences in the peak position in the spectrum.

TABLE II
REAL PARTS OF DIELECTRIC PERMITTIVITY AND LOSSES FOR DIFFERENT OIL SAMPLES

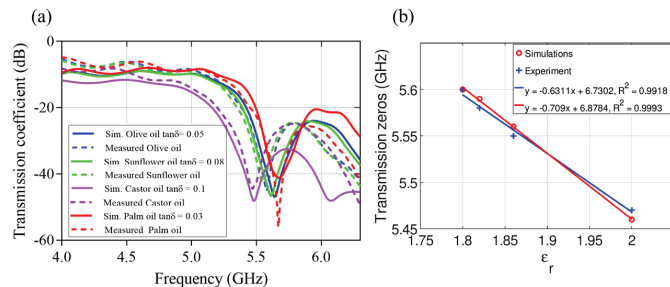| Oil sample	ε'	$\tan \delta$
Palm oil	1.8 [20]	0.03
Olive	1.82 [21]	0.05
Sunflower	1.86 [22]	0.08
Castor	2 [23]	0.1

Fig. 5.   Comparison of simulated and measured results for palm, olive, sunflower and castor oils. (a) Positions of transmission zeros in the spectrum, (b) Linearity of transmission zero positions for different oil samples.

IV.   CONCLUSION

In this paper, we proposed a SSPP-based microwave sensor optimized for liquid analytes with a low dielectric constant. The proposed SSPP-based sensor was optimized for excellent linear properties and very high sensitivity. The sensor was realized in rapid fabrication technology that uses low-cost, and transparent materials, and a combination of xurography and laser micromachining. In that sense, the proposed sensor showed a big sensing potential of SSPP structures and offered a rapid and simple fabrication solution for highly sensitive applications. In addition, by changing unit cell dimensions, the proposed sensor can be adapted for food quality control, control of petroleum products, and biomedical applications.

REFERENCES

[1] N. K. Tiwari, S. P. Singh, and M. J. Akhtar, "Novel Improved Sensitivity Planar Microwave Probe for Adulteration Detection in Edible Oils", *IEEE Microw. Wireless Compon. Lett.*, vol. 29, no. 2, pp. 164–166, Feb. 2019.

[2] M. Liu, X. Qin, Z. Chen, L. Tang, B. Borom, N. Cao, D. Barnes, K. Cheng, J. Chen, T. Wang, and J. Rao, "Frying Oil Evaluation by a Portable Sensor Based on Dielectric Constant Measurement", *Sensors (Basel)*, vol. 19, no. 24, Dec. 2019.

[3] Z. Li, Q. Xue, Q. Wang, H. Zhang, and X. Duan, "Biomolecules Detection Using Microstrip Sensor with Highly-Ordered Nanowires Array", *2019 IEEE SENSORS*, 2019, pp. 1–4.

[4] A. S. Zapasnoy, V. P. Belichenko, V. P. Yakubov, A. V. Gorst, A. S. Mironchev, A. V. Klokov, and K. V. Zavyalova, "Application of broadband Microwave Near-Field Sensors for Glucose Monitoring in Biological Media", *Appl. Sci.*, vol. 11, no. 4, p. 1470, Feb. 2021.

[5] I. Podunavac, V. Radonic, V. Bengin, and N. Jankovic, "Microwave Spoof Surface Plasmon Polariton-Based Sensor for Ultrasensitive Detection of Liquid Analyte Dielectric Constant", *Sensors*, vol. 21, no. 16, p. 5477, Aug. 2021.

[6] N. Cselyuszka, Z. Sakotic, V. Crnojevic-Bengin, V. Radonic, and N. Jankovic, "Microwave Surface Plasmon Polariton-Like Sensor Based on Half-Mode Substrate Integrated Waveguide for Highly Sensitive Dielectric Constant Detection", *IEEE Sens. J.*, vol. 18, no. 24, pp. 9984–9992, Dec. 2018.

[7] X. Bao, I. Ocket, G. Crupi, D. Schreurs, J. Bao, D. Kil, B. Puers, and B. Nauwelaers, "A Planar One-Port Microwave Microfluidic Sensor for Microliter Liquids Characterization", *IEEE J. Electromagn. RF Microw. Med. Biol.*, vol. 2, no. 1, pp. 10–17, Mar. 2018.

[8] V. Radonić, S. Birgermajer, I. Podunavac, M. Djisalov, I. Gadjanski, and G. Kitić, "Microfluidic Sensor Based on Composite Left-Right Handed Transmission Line", *Electronics*, vol. 8, no. 12, p. 1475, Dec. 2019.

[9] N. Jankovic and V. Radonic, "A Microwave Microfluidic Sensor Based on a Dual-Mode Resonator for Dual-Sensing Applications", *Sensors (Basel)*, vol. 17, no. 12, Nov. 2017.

[10] J. Zhang, L. Zhang, and W. Xu, "Surface plasmon Polaritons: Physics and Applications", *J. Phys. D, Appl. Phys.*, vol. 45, no. 11, p. 113001, Mar. 2012.

[11] N. Gomez-Cardona, E. Reyes-Vera, and P. Torres, "High Sensitivity Refractive Index Sensor Based on the Excitation of Long-Range Surface Plasmon Polaritons in H-Shaped Optical Fiber", *Sensors (Basel)*, vol. 20, no. 7, Apr. 2020.

[12] Y. Wang, S. Li, Y. Guo, S. Zhang, and H. Li, "Surface Plasmon Polariton High-Sensitivity Refractive Index Sensor Based on MMF-MOF-MMF Structure", *Infrared Phys. Technol.*, vol. 114, p. 103685, May 2021.

[13] S. Joseph, S. Sarkar, and J. Joseph, "Grating-Coupled Surface Plasmon-Polariton Sensing at a Flat Metal-Analyte Interface in a Hybrid-Configuration", *ACS Appl. Mater. Interfaces*, vol. 12, no. 41, pp. 46519–46529, Oct. 2020.

[14] Y. Peng, Y. Zhao, X. Hu, and Y. Yang, "Optical Fiber Quantum Biosensor Based on Surface Plasmon Polaritons for the Label-Free Measurement of Protein", *Sensors and Actuators B: Chemical*, vol. 316, p. 128097, Aug. 2020.

[15] S. E. Swiontek, D. P. Pulsifer, and A. Lakhtakia, "Optical Sensing of Analytes in Aqueous Solutions with a Multiple Surface-Plasmon-Polariton-Wave Platform", *Sci. Rep.*, vol. 3, p. 1409, 2013.

[16] J. B. Pendry, L. Martín-Moreno, and F. J. Garcia-Vidal, "Mimicking Surface Plasmons with Structured Surfaces", *Science*, vol. 305, no. 5685, pp. 847–848, Aug. 2004.

[17] X. Chen and W. Fan, "Ultrasensitive Terahertz Metamaterial Sensor Based on spoof Surface Plasmon", *Sci. Rep.*, vol. 7, no. 1, p. 2092, May 2017.

[18] G. Liu, D. Cheng, B. Zhang, G. Shu, and J. Wang, "A Microwave Biosensor Based on Spoof Surface Plasmon Polaritons for *In Vivo* Measurement of the Water Content of Human Skin Tissues", *J. Phys. D, Appl. Phys.*, vol. 52, no. 20, p. 205401, May 2019.

[19] L. Liu and D. Jiang, "A Microwave Detector Based on Spoof Surface Plasmon Polaritons Structure", *AIP Adv.*, vol. 11, no. 3, p. 035008, Mar. 2021.

[20] M. A. Sairin, N. N. A. Nizar, S. A. Aziz, and F. Z. Rokhani, "Study of Dielectric Permittivity and Fatty Acid Composition for Fats and Oil in Wide Frequency Spectroscopy Measurement at 0.5–50 GHz", *2016 10th International Conference on Sensing Technology (ICST)*, 2016, pp. 1–5.

[21] A. A. Sonkamble, R. P. Sonsale, M. S. Kanshette, K. B. Kabara, K. H. Wananje, A. C. Kumbharkhane, and A. V. Sarode, "Relaxation Dynamics and Thermophysical Properties of Vegetable Oils Using Time-Domain Reflectometry", *Eur Biophys J*, vol. 46, no. 3, pp. 283–291, Apr. 2017.

[22] X.-Q. Xu, V. H. Tran, M. Palmer, K. White, and P. Salisbury, "Chemical and Physical Analyses and Sensory Evaluation of Six Deep-Frying Oils", *J Am Oil Chem Soc*, vol. 76, no. 9, pp. 1091–1099, Sep. 1999.

[23] N. A. Ibrahim and M. A. A. Zaini, "Microwave-Assisted Solvent Extraction of Castor Oil From Castor Seeds", *Chin. J. Chem. Eng.*, vol. 26, no. 12, pp. 2516–2522, Dec. 2018.